Three-dimensional mesoscale modelling of multi-span masonry arch bridges subjected to scour

Enrico Tubaldi[1], Lorenzo Macorini[2], Bassam A Izzuddin[3]

Department of Civil and Environmental Engineering, Imperial College London, South Kensington Campus, London, UK

[1]Marie Curie Research Fellow, Email: e.tubaldi @imperial.ac.uk (corresponding author)

[2] Senior Lecturer, Email: l.macorini@imperial.ac.uk

[3] Professor of Computational Structural Mechanics, Email: b.izzuddin@imperial.ac.uk

Keywords: masonry arch bridges; scour; nonlinear analysis; 3D modelling; mesoscale description; settlements.

Abstract

Many masonry arch bridges cross waterways and are built on shallow foundations which are often submerged and exposed to the scouring action of the stream. The limited resistance of masonry arch bridges to foundation settlements makes them very vulnerable to scour and calls for the development of advanced tools for evaluating and improving the capacity against this flood-induced effect. This paper describes a novel three-dimensional modelling strategy for describing the behaviour of multi-span masonry arch bridges subjected to scour at the base of the pier shallow foundations. A mesoscale description is employed for representing the heterogeneous behaviour of masonry units, mortar joints and brick-mortar interfaces, whereas a domain partitioning approach allowing for parallel computation is used to achieve computational efficiency. The scouring process is described via a time-history analysis in which the elements representing the soil are progressively removed from the model according to a specific scour evolution. The proposed modelling approach is first employed to simulate available experimental tests on a dry masonry wall subjected to the settlement of the bearing system and on a reduced scale brick-masonry bridge specimen subjected to scour-induced pier settlements. Subsequently, a numerical example consisting of a multi-span arch bridge subjected to the scouring action is presented to illustrate the potential of the proposed modelling approach and its capabilities for evaluating the vulnerability and risk of masonry arch bridges under flood scenarios.

1. Introduction

Masonry arch bridges are durable, sustainable, and aesthetically appealing structures forming a significant portion of the bridge stock of Europe [1],[2]. Many masonry arch bridges span rivers and have their substructures, either piers or abutments or both, founded in the river bed. This exposes them to different flood-induced actions, including hydrodynamic pressure on the submerged surfaces, buoyant forces reducing the effective unit weights of submerged components, impact of lumps/debris [3]. More importantly, water flow results in scour at the footings of piers and abutments, which is the most common cause of collapse due to the high vulnerability of arches to foundation settlements [4],[5]. Given the high number of masonry-arch bridges and their socio-economic and cultural heritage value, the accurate prediction of their capacity against scour is a task of paramount importance.

In the last decades, intensive research has been carried out to develop models capable of simulating the complex behaviour and interaction of the components of masonry arch bridges, including the arch barrel, the backfill, the lateral walls, and the piers and abutments. In particular, various numerical models of different degree of complexity have been proposed for the collapse analysis of arch bridges under combined permanent and traffic loads (see Zhang *et al.* [6] and Sarhosis *et al.* [7] for a state of the art review). Despite the numerous experimental and numerical studies carried out to date, there are still several open issues in the analysis of masonry arch bridges. First of all, most of previous experimental and numerical studies have focused on single span masonry arches whereas many bridges consist of multiple spans. Thus, the presence of the substructures with their foundations and their interaction with the superstructure has yet to be fully explored. Moreover, numerical models have seldom considered the three-dimensional (3D) nature of the problem, which is important even in the case of vertical patch loading ([8]-[10]). Finally, no modelling strategies have been proposed thus far for describing the vulnerability of masonry arch bridges to scour. In this respect, it should be observed that arch bridges are often built on shallow footings, and that many procedures for scour risk assessment ([11],[12]) assume that the bridge collapses when the maximum scour depth reaches the level of the foundation base. However, given the complexity of the problem, the non-symmetric shape of the scour hole, and the bridge redundancy, a 3D structural analysis of the soil-foundation-bridge domain is required to evaluate fully the effects of scour. To date, only a few works have investigated the effect of scour on bridges by performing a full analysis of the soil-foundation-bridge domain (e.g. [13]-[15]). However, these studies address bridges with pile foundations. Thus, there is a

significant need for numerical models that allow the investigation of masonry arch bridges with shallow foundations.

Previous work at Imperial College proposed a mesoscale approach [16] for evaluating the behaviour of masonry arches [10] and single-span masonry arch bridges [17], under vertical loading. This advanced modelling strategy, implemented in ADAPTIC [18] and validated against experimental results, allows for an accurate bridge response prediction, as it takes into account the 3D nature of the problem and important features of masonry arches such as the masonry bond, the spandrel walls contribution, and the arch-backfill interaction. Moreover, although the proposed modelling strategy is computationally expensive, significant reduction of the computational cost can be gained in the numerical simulations by coupling the proposed modelling strategy with the hierarchic partitioning approach allowing for parallel computation developed previously at Imperial College [19]-[21].

This paper illustrates the extension of this modelling strategy to the analysis of multi-span bridges under different types of flood-induced loadings which require the consideration of the 3D nature of the problem and the interaction between the superstructure, the piers and the bridge foundations. Firstly, the capability of the proposed modelling approach to describe the collapse mechanism induced by settlements is investigated by simulating an experimental test carried out on a simple masonry wall with dry bricks [22]. Subsequently, the results of the test on a 1/2 scale model of a two-span bridge conducted at Polytechnic University of Turin [23] are considered and simulated by developing a numerical model of the bridge. In the test, the bridge was subjected to translational plus rotational settlements at the base of the pier foundations to represent the undermining of the foundation due to scour.

In the second part of the paper a realistic model of a two span bridge similar to Copley Bridge in Yorkshire, which recently collapsed because of pier scour, is developed together with the foundations and the soil domain represented by using the Winkler approach. The effect of scour is described by performing a time-history analysis where the elements defining the soil are progressively degraded, which allows the combined modelling of both the loss of support and the settlements due to scour. The proposed modelling approach enables the representation of the complex 3D mechanism which often characterises the failure of masonry arch bridges subjected to pier scour and can be conveniently employed in more general frameworks and procedures for flood risk assessment and mitigation [24].

2. Modelling strategy for multi-span brick-masonry arch bridges subjected to scour

This section describes the finite element (FE) modelling approach and analysis procedure for describing the 3D behaviour of masonry arch bridges subjected to foundation scour. The proposed approach extends and advances the models originally developed at Imperial College for the analysis of large-scale unreinforced masonry walls [16],[25], and for the evaluation of arches [10] and single-span masonry arch bridges [17] subjected to vertical loadings. In particular, the previous single-span bridge models are extended here to consider multi-span bridges, accounting further for the behaviour of the substructures and the foundations, as well as the interaction between the soil and the foundation, which is essential for simulating the effects of scour (Fig. 1).

The next sub-sections describe in detail the modelling approach for the bridge components, the hierarchic partitioning strategy for speeding up the bridge analysis, and the strategy for describing the effects of scour.

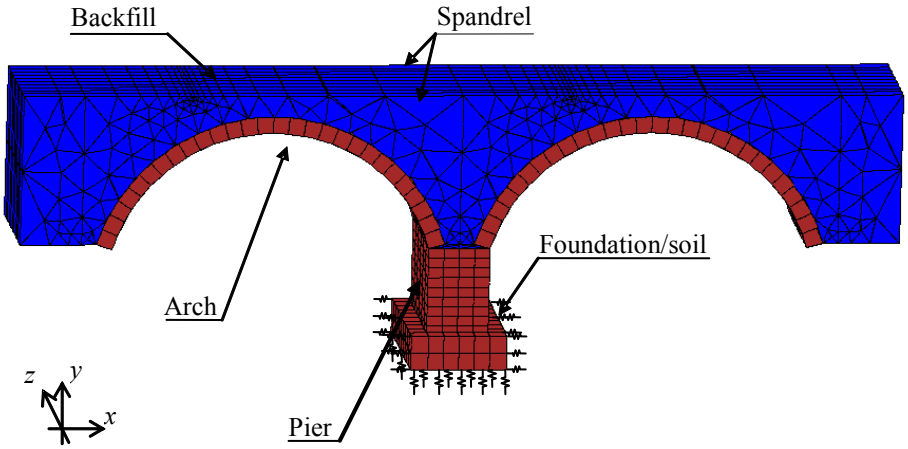

Fig. 1. Bridge-foundation-soil model and Winkler-type interfaces.

2.1 3D model of the bridge

Masonry is a heterogeneous and strongly nonlinear material whose behaviour depends on the orientation of the loading direction with respect to the masonry bond, where mortar joints represent preferential fracture planes [26]. In this respect, a detailed mechanical model for the masonry arch and piers should take into account not only the mechanical characteristics of units and mortar but also the actual 3D masonry texture. Unlike continuous approaches which assume masonry a homogeneous material [9][27], a discrete modelling strategy is employed to represent the actual masonry bond and model the development of cracks in real

brick/stone-masonry arches and piers. This numerical strategy allows for an accurate description of the 3D domain of any masonry arch/pier, as the actual 3D masonry bond is represented using two or more elastic solid elements for each brick and 2D nonlinear interface elements for mortar joints. In particular, 20-noded elastic solid elements formulated according to standard FE procedures are used together with specific 2D zero-thickness nonlinear interface elements with 16 nodes accounting for material and geometric nonlinearity. In this way, the typical fracture surfaces which characterise the nonlinear response up to collapse of masonry arches can be represented. These correspond to radial cracks, circumferential cracks leading to ring separation in multi-ring arches and longitudinal cracks caused by transverse bending. While the first two types of crack generally take place in the mortar joints, longitudinal cracks may pass also through the masonry units. Thus nonlinear interface elements are placed also in the middle of each brick to capture the potential development of cracks. This renders the FE mesh for brick-masonry arches relatively simple, as it is made up of identical solid elements connected to each other by nonlinear brick-brick and mortar interface elements as shown in Fig. 2. Material nonlinearity is taken into account by employing for the interface elements a cohesive model, which enables an effective representation of damage, cracks and plastic separations [16]. In particular, the latest refinement of the interface model, based on the concept of coupled plasticity and damage and described in detail in [28], is employed to increase the computational robustness of the local plastic problem. A multi-surface yield criterion in the stress domain governs the development of permanent plastic strains, while strength and stiffness degradation are captured through the evolution of an anisotropic damage tensor, defined by three scalar damage variables: D_{nt} for the normal direction in tension, D_{nc} for the normal direction in compression, and D_s for the two tangential directions.

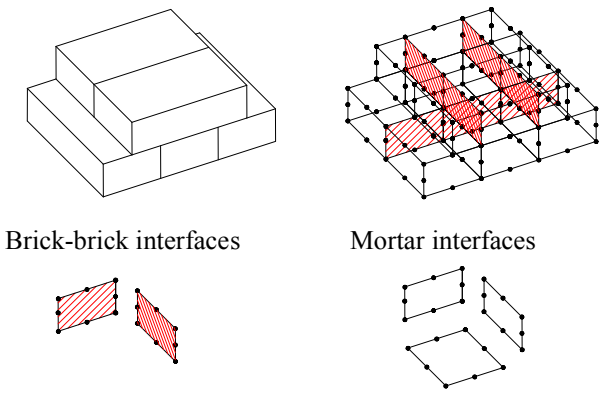

Fig. 2. Portion of a brick wall with flemish bond and relevant FE modelling.

A realistic representation of the fill behaviour and its interaction with the arch barrel is essential for an accurate response prediction of masonry arch bridges [27],[29]. In the proposed modelling strategy, the backfill domain is discretised using 15-noded elasto-plastic tetrahedral elements. Similar to other studies on masonry arch bridges [8],[9],[27] these elements are characterised by an elasto-plastic material behaviour. The isotropic elastic response is described adopting specific values for the Young's modulus and Poisson's ratio, whereas the plastic behaviour is modelled by employing a modified Drucker-Prager (D-P) yield criterion, with a tension and compressive caps as described in [30]. Fig. 3a illustrates the multi-surface yield-criterion in the $I_1 - \sqrt{J_2}$ plane, where I_1 and J_2 represent respectively the first invariant of the stress tensor and the second deviatoric stress invariant, I_{1t} denotes the tensile limit for the first invariant of stresses, and $\chi(\kappa)$ and κ describe the limit of the compressive elliptic cap. A hardening behaviour is associated with the smooth elliptic cap in compression and the variations of $\chi(\kappa)$ and κ are controlled by the volumetric part of the plastic deformation [30]. This is generally considered for describing potential compaction phenomena in the backfill (i.e., irreversible decrease in volume under pressure). A non-associative flow rule is employed to avoid excessive dilatancy. The equations describing the D-P yield surface and relevant plastic potential read:

$$F_1(\xi,\rho) = \sqrt{6}\alpha\xi + \rho - \sqrt{2}k = 0 \tag{1}$$

$$G_1(\xi,\rho) = \sqrt{6}\alpha_d\xi + \rho - \sqrt{2}k_d = 0 \tag{2}$$

where $\xi = \frac{1}{\sqrt{3}} I_1$ and $\rho = \sqrt{2J_2}$.

The D-P yield envelope is a smooth version of the Mohr–Coulomb (M-C) yield surface, and its parameters α and k can be expressed in terms of the cohesion c and the friction angle ϕ related to the M-C yield surface. In particular, the values of α and k can be chosen to make the D-P yield envelope coincident either at the outer edges or at the inner edges of the M-C yield surface (Fig. 3b) [31]. Coincidence at the inner edges is usually recommended, and it is obtained by employing the following expressions to calculate α and k:

$$\alpha = \frac{2\sin(\phi)}{\sqrt{3}(3+\sin(\phi))} \;;\; k = \frac{6c\cos(\phi)}{\sqrt{3}(3+\sin(\phi))} \tag{3}$$

173 The values of α_d and k_d can be evaluated by replacing the friction angle ϕ in Eqn. (3) with
174 the dilatancy angle ϕ_d.

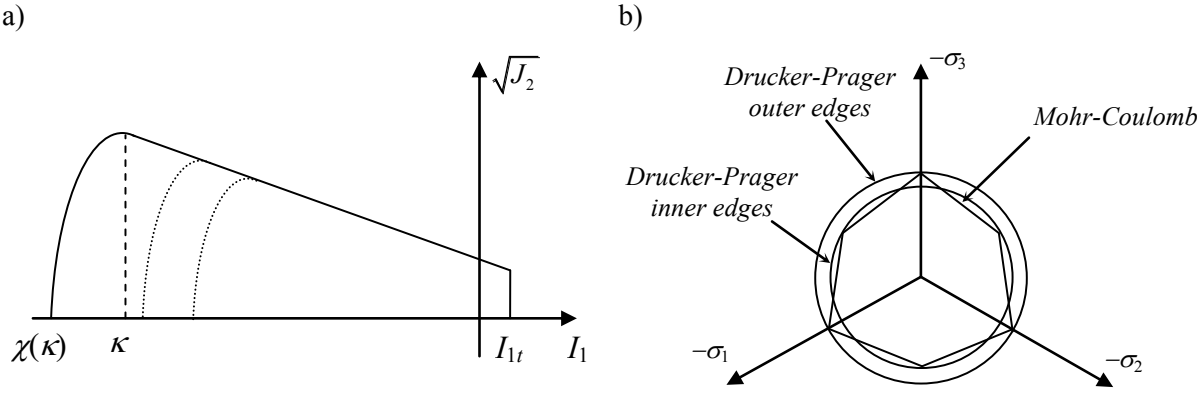

175 Fig. 3. a) Modified D-P model with tensile cap and elliptic cap in compression, b) fitting of the D-P yield
176 surface to the M-C yield surface in the octahedral plane.

177 In the proposed modelling approach for masonry arch bridges, the spandrel walls are also
178 discretised using 15-noded elasto-plastic tetrahedral elements. This is a practical modelling
179 strategy, as it enables the representation of the masonry spandrel walls using the same FE
180 mesh characteristics employed for the backfill. A more detailed description would require the
181 use of the masonry mesoscale model employed for the arches and the piers which, in the case
182 of the spandrel walls, leads to some complexity in the mesh generation thus it has not been
183 considered in this study. A coupled elasto-plastic damage model is employed to describe the
184 constitutive law for the solid elements of the spandrel walls, where the following relationship
185 between the stress vector $\{\sigma\}$ and the strain vector $\{\varepsilon\}$ is adopted:

186 $$\{\sigma\} = (1-\omega)[D]\left(\{\varepsilon\} - \{\varepsilon_p\}\right) \tag{4}$$

187 in which $\{\varepsilon_p\}$ denotes the plastic deformations as per the previous yield criterion and flow
188 rule, $[D]$ is the elasticity matrix, and ω is the damage parameter which varies between 0
189 (undamaged case) and 1 (fully damaged case). This damage parameter is used to control the
190 softening branch following the formation of cracks in masonry or the attainment of the
191 compression resistance. The evolution of ω is controlled by the plastic work done by the
192 stresses, whose increment is given by:

193 $$\begin{aligned} &dW_{pl,1} = \langle\sigma\rangle\{d\varepsilon_p\},\ dW_{pl,2} = 0 \qquad I_1 \geq \kappa \\ &dW_{pl,2} = 0 \quad dW_{pl,2} = \langle\sigma\rangle\{d\varepsilon_p\} \qquad I_1 < \kappa \end{aligned} \tag{5}$$

The damage parameter is expressed as:

$$\omega = 1-\left(1-D_c\right)\left(1-D_t\right) \tag{6}$$

where:

$$D_c = 1-\exp\left(\frac{-W_{pl,2}}{G_{f,II}}\right),\ D_t = 1-\exp\left(\frac{-W_{pl,1}}{G_{f,I}}\right) \tag{7}$$

and where $G_{f,I}$ and $G_{f,II}$ represent fracture energies for tension-shear mode and for compression mode respectively.

A mortar mesh tying method for non-conforming interfaces is employed to enhance the efficiency of the computational strategy. This method [17] allows the backfill and the arch barrel domains to be meshed independently without compatibility considerations, thus enabling the optimization of the individual meshes. In particular, a coarser mesh can be employed at the arch barrel-backfill interface, without compromising the accuracy of the results [17]. The interaction between the arch and the backfill is described by employing nonlinear interface elements to represent separation and frictional sliding at the arch-backfill physical interface. These interface elements connect the set of nodes at the extrados of the arch barrel with a set of coincident nodes, which are then tied to the nodes at the intrados of the backfill.

With reference to the foundations and the soil, masonry arch bridges are often built on shallow foundations [1],[32],[33], making them very vulnerable to scour. In order to simulate the scour effects, the bridge model should also include the foundation and the surrounding soil. The soil medium has very complex mechanical behaviour, which is generally nonlinear, stress-dependent, anisotropic and heterogeneous in nature. The difficulty of simulating these features may outweigh the advantages of using complex modelling approaches. Thus, in this study, a simplified Winkler subgrade modelling approach is employed to investigate the effects of scour, where the soil domain is described by using interface elements surrounding the foundation (Fig. 1b). Although this approach is approximate, it has the advantage of limiting the computational cost of the analysis, which is already very high due to the mesoscale description employed for the masonry component. Moreover, the purpose of this study is to illustrate a procedure for evaluating the effect of scour on masonry arch bridges, rather than evaluating the actual values of the scour depths that lead to bridge failure.

Nevertheless, the proposed strategy can still be employed in conjunction with more sophisticated soil models, if available.

According to this simplified approach, the soil interfaces can resist only normal compressive forces and their behaviour is linear elastic and described by the coefficient of subgrade reaction k_s, providing the relationship between deflection (settlement) and soil pressure [34],[35]. The value of the subgrade parameter depends on the footing size and can be estimated on the basis of plate load tests or through analytical expression allowing for the soil characteristics. In this regard, different equations can be found in the literature for calculating k_s, and different values should be chosen for the subgrade parameter along the vertical and horizontal directions.

In this study, the subgrade reaction in the vertical direction is taken as $k'_{sv} = \frac{k_{sv}}{BL}$, where k_{sv} denotes the vertical translational impedance of a rigid foundation of length L and width B, with $L > B$. A specific expression for k_{sv} has been developed by Gazetas [36] as a function of the shear modulus of the soil G_s and of the foundation geometry [37]. It is worth noting that the proposed approach generally underestimates the rotational stiffness of the soil-foundation system [38], but the error is expected to lead to conservative results (e.g., overestimation of settlements). Additionally, the soil layer above the foundation is assumed to provide a contribution in term of weight but not of stiffness.

The value of the subgrade reactions along the horizontal directions x and z can be evaluated as $k'_{sh,x} = k_{sh,x} / A_x$ and $k'_{sh,z} = k_{sh,z} / A_z$. These expressions are obtained by distributing uniformly along the lateral foundation surfaces A_x and A_z the horizontal impedances $k_{sh,x}$ and $k_{sh,z}$, whose expressions are given by Gazetas [36].

Alternatively, the relationship provided by Terzaghi [34] and valid for cohesionless soils can be considered:

$$k_h = \frac{n_h y}{b} \tag{8}$$

where y is the depth, b is the dimension of the foundation perpendicular to the direction of the displacement, n_h is a parameter that depends on the density of the sand and ranges from 0.0014 N/mm^3 for very loose sand to 0.0118 N/mm^3 for dense sand in submerged conditions according to [34],[39]. Higher values are however reported in [40].

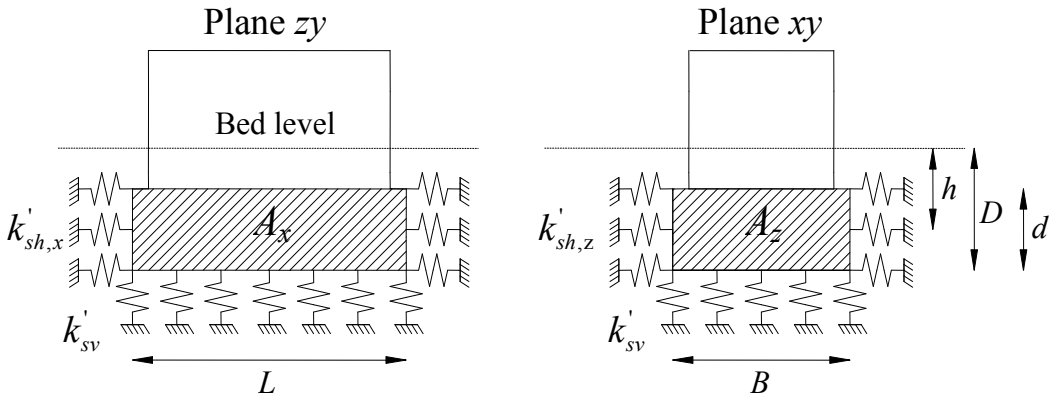

252

253 Fig. 4. Modelling of Winkler-type interfaces for soil-structure interaction.

254 **2.2 Partitioning strategy description**

255 A hierarchical partitioned modelling strategy recently developed at Imperial College [19]-[21]
256 is employed to speed up the computations. This is particularly beneficial for the mesoscale
257 analysis of large masonry structures [25], where the use of monolithic simulations generally
258 leads to excessively long computational times. This approach consists of replacing the
259 original model with a parent structure which comprises super-elements representing the
260 partitioned subdomains. Each super-element corresponds to one partition, and the number of
261 element nodes connected to the parent structure is equal to the number of nodes at the
262 partitioned boundary in the partition that it represents. Each partition is then modelled using
263 the detailed 3D mesoscale description, while the parent structure corresponds to the
264 partitioned boundary. Dual super-elements allow for partitions to be modelled as separate
265 processes, where communication between each parent/child superelement pair ensures that
266 the analysis for all partitions is run in parallel. The hierarchic approach [19] for model
267 partitioning is a further enhancement of the original partitioning technique described in [21].
268 It allows multi-level partitions, where generic partitions can be further subdivided by
269 replacing their parts with partition super elements. In this way, the removed parts can be
270 modelled at further lower levels of partitioning. Fig. 5 shows an example of hierarchic
271 partitioning for a two-span bridge model. In particular, Fig. 5a depicts the whole model
272 together with the child partitions at the lowest level and the boundaries (in red) whose nodes
273 form the parent domain. Fig. 5b illustrates the hierarchic partitioning of the arch, the backfill,
274 and the pier. A semi-automatic mesher has been developed at Imperial College [41] to
275 generate the FE mesh with partitions.

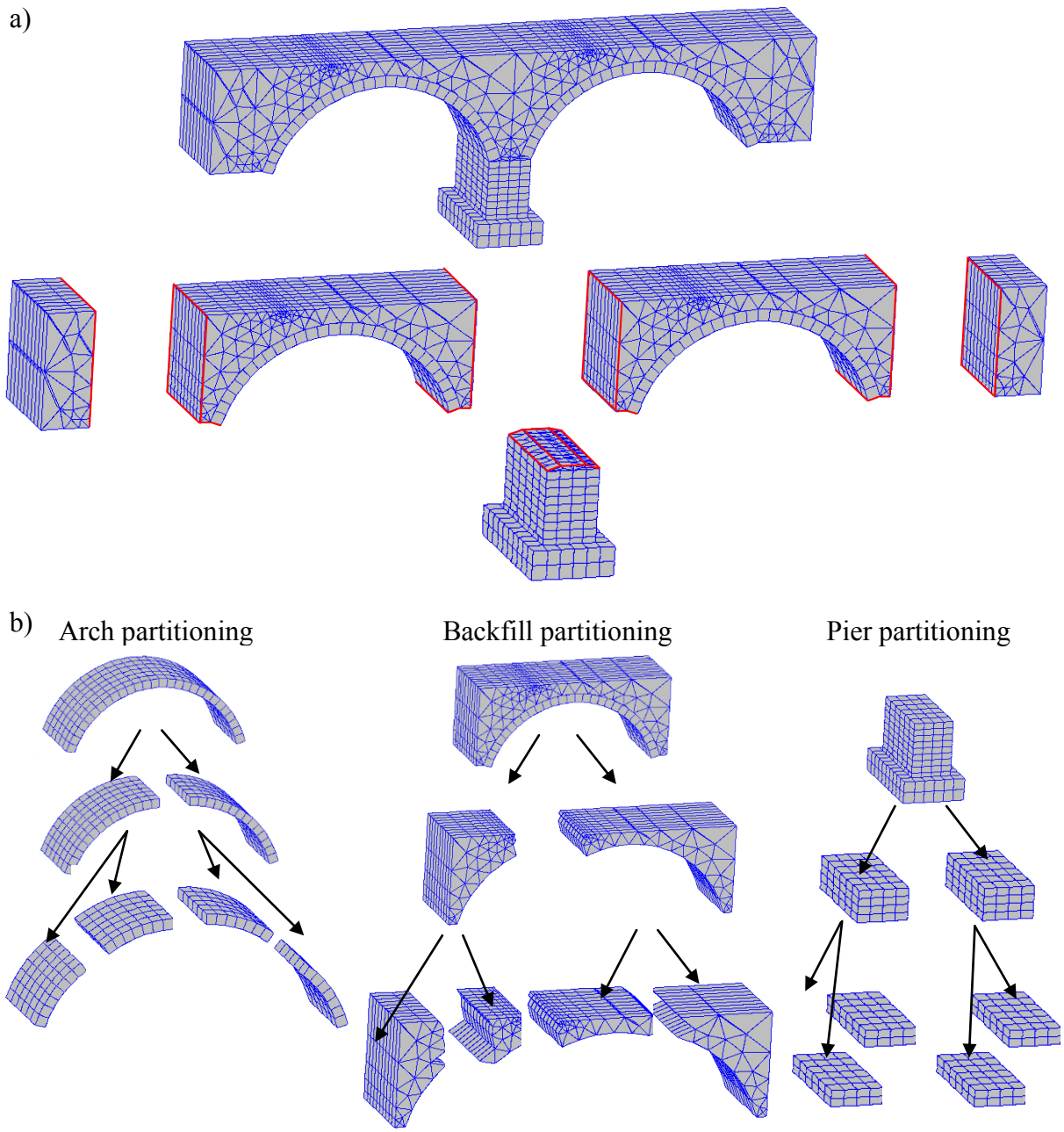

Fig. 5. Model partitioning example: a) decomposition of the multi-span bridge domain, b) decomposition of the bridge component for each span.

2.3 Simulation of scour effects

Scour is a natural phenomenon caused by erosion or removal of streambed or bank material from bridge foundations due to flowing water [42],[43]. This phenomenon occurs continuously over time but it is particularly relevant in the event of a flood, during which the water has more energy to transport material downstream. In the literature, it is generally agreed that there are three types of scour: degradation scour, contraction scour and local scour [5] which may generally occur simultaneously at a particular site. Examining the types of scour in more detail, degradation scour represents the previously mentioned case, where

the cumulative effect of the phenomenon is significant for the stability of a bridge pier. Specifically, this type of scour simply involves the removal of sediment by the river flow, leading to the lowering of the river bed. Contraction scour is the removal of sediment caused by the approaching flow which increases in speed as it moves through a bridge opening that is narrower than natural river channel. Last, local scour is the removal of sediment by a vortex system forming due to the obstruction to the main flow from the bridge piers or the abutments. This study focuses on the effects of local scour only. In order to simulate these effects, it is necessary to define a model for the spatial and temporal variation of the geometric properties of the scour hole, which controls the loss of soil supporting the foundations. Many experimental studies have analysed the shape of the scour hole [44]-[46], but its specific geometrical characteristics cannot be accurately established *a priori* for all the piers and foundation geometries, and experimental results generally show significant scatter. Thus, for the sake of simplicity, a constant inverted pyramidal scour form is considered in this study (Fig. 6). The vertex of the pyramid is assumed along a vertical line passing through the centre of the upstream face of the pier, the upstream slope of the hole is taken equal to angle of repose of the soil, whereas the downstream slope is approximately half that upstream, consistently with [43]. It is also assumed that the scour hole slope in the direction perpendicular to the flow is 5/6 of that upstream, as in [47]. Having considered a fixed shape of the scour hole, the hole geometry is defined by a single parameter, which is the maximum scour depth y_s, identifying the scour hole vertex.

In Witzany *et al.* [33], the effects of scour on bridge structures are described in terms of settlements inducing the subsidence, shifting, or partial turning of the pier foundations. However, only an analysis of the soil-foundation-bridge system, simulating the progressive removal of the soil surrounding the foundations due to scour, can quantify these settlements and establish whether they consist of pure rotation or of translation plus rotations. For this purpose, in this study the effects of scour are simulated by progressively reducing the stiffness (and thus the resisting force) of the elements representing the soil surrounding the foundation. Different discrete levels of the scour maximum depth are considered, and for each depth the scour hole geometry is determined based on the previously discussed assumption. The depth of the centroid of each element (either interfaces or solid elements) representing the soil is compared with the depth of scour at the same location. If the element centroid is below the scour threshold, its resisting force and stiffness are reduced to zero. Fig. 6 illustrates the development of the scour hole at three different stages of scour, together with

the corresponding models. In order to simulate the evolution in time of the scouring process and the deepening of the scour hole up to the chosen maximum scour depth, a time history analysis is carried out and the degradation of the stiffness of the soil elements is assumed to occur in more than one time step to smooth the process. It is worth noting that the influence of the removal of an upper soil layer (i.e., scouring) on the stiffness of the lower soil layer is disregarded in the model.

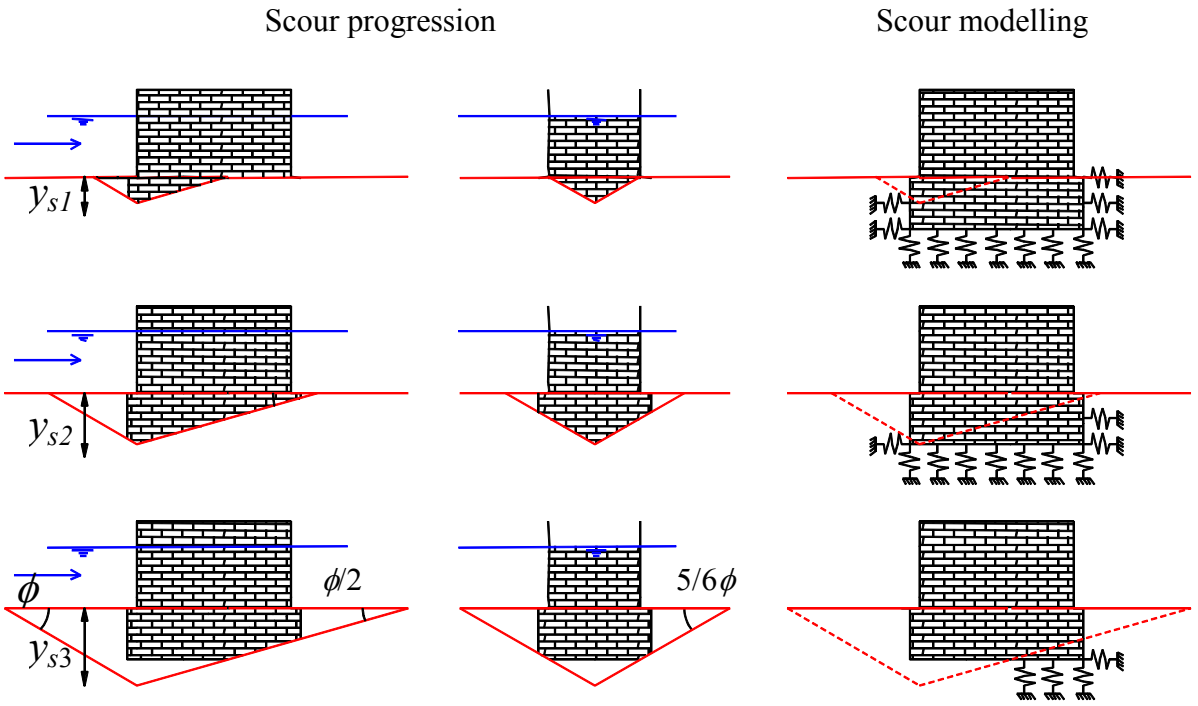

Fig. 6. Assumed scour hole shape and scour progression modelling in the case of soil modelled with Winkler-type interfaces.

3. Numerical simulation of a masonry wall subjected to settlements

In order to demonstrate the capability of the proposed mesoscale modelling strategy for masonry structures representing the effects of foundation settlements, the experimental test described in [22] is simulated in ADAPTIC [18]. The tested specimen consists of a wall with 1100 mm width, 400 mm height, and 100 mm thickness, made of dry jointed tuff masonry blocks with dimensions of 200×100×50 mm^3. The wall includes five-and-half bricks along the horizontal direction, and eight bricks along the vertical direction. The first three bricks at the base of the wall from the left are supported on a fixed foundation, whereas the other two-and-half bricks lay on a support system which allows the application of vertical settlements. Rolling bearings located on the movable bearing system enables horizontal displacements at the support. Fig. 7a shows the wall model, where only one 20-noded solid element is used per half brick, such that two interface elements are employed for each bed joints with only one

342 interface element for each head joint and for modelling potential vertical cracks at the mid-
343 plane of the bricks (brick-brick interface). The unit weight of the tuff bricks is 12.0 kN/m^3,
344 resulting in a total weight of the panel of 528 N. Zero cohesion and tensile resistance are
345 assumed for mortar interfaces together with a friction coefficient of 0.4 to simulate dry brick
346 conditions.

347 Fig. 7b shows the relationship between the imposed vertical displacement δ and the sum of
348 the reaction forces at the movable support nodes R. The initial value of R is very close to the
349 weight of the wall above the support, and it decreases very fast by increasing δ until it
350 reaches a value of about 106N. This predicted residual value of the resistance is close to the
351 experimental one, but it is reached in the numerical model for smaller displacements when
352 compared to the physical response.

353 Fig. 8a shows the deformed shape of the wall for a value of δ= 10mm. The deformation
354 mechanism involves sliding and rocking of the middle part of the wall panel and the
355 movement of a trapezoidal macro-block of 15 half bricks over the movable support, which
356 translates downwards and in horizontal direction. The failure mechanism predicted by the
357 numerical model is in a good agreement with experimental results, as a very similar cracking
358 pattern has been observed in the physical test [22]. It is noteworthy that the final value of the
359 reaction force R, i.e., about 100 N, is slightly higher than the weight of 15 half bricks, i.e., 90
360 N. This is because it equilibrates not only the weight of the macro-block, but also the vertical
361 force transmitted from the central macro-block at the contact point, located at the top-right.
362 Eventually, by increasing further the displacement, the value of R would further reduce.

363 In order to highlight the differences between scour, i.e., erosion of the material surrounding
364 the foundation, and settlements, the procedure for simulating scour described in the previous
365 section is applied to the same wall model. A set of interfaces is introduced at the base of the
366 wall, in correspondence of the movable support, and the resisting force and normal stiffness
367 of these interfaces are progressively reduced to zero to simulate the loss of the foundation
368 support. The relation between the sum of the reaction forces R at the base of the interfaces
369 subjected to scour and the maximum vertical displacement δ is shown in Fig. 7b, and the
370 corresponding mechanism observed at the end of the scour process, when R approaches 0 kN
371 and the bottom corner of masonry would fall away, is illustrated in Fig. 8b. It can be observed
372 that the force-displacement curve is very steep compared to the curve obtained by imposing
373 the settlement. In particular, by simulating the scour process, the sum of the reaction forces R

drops to zero for very low values of the displacement δ. On the other hand, under imposed settlements, R decreases gradually for increasing values of δ, until it reaches a stable value. Moreover, some differences are observed in the cracking mechanisms due to the applied settlement or scour. In particular, scour results in a non-uniform displacement pattern at the wall base which cannot be known a priori and can be unveiled by applying the proposed procedure.

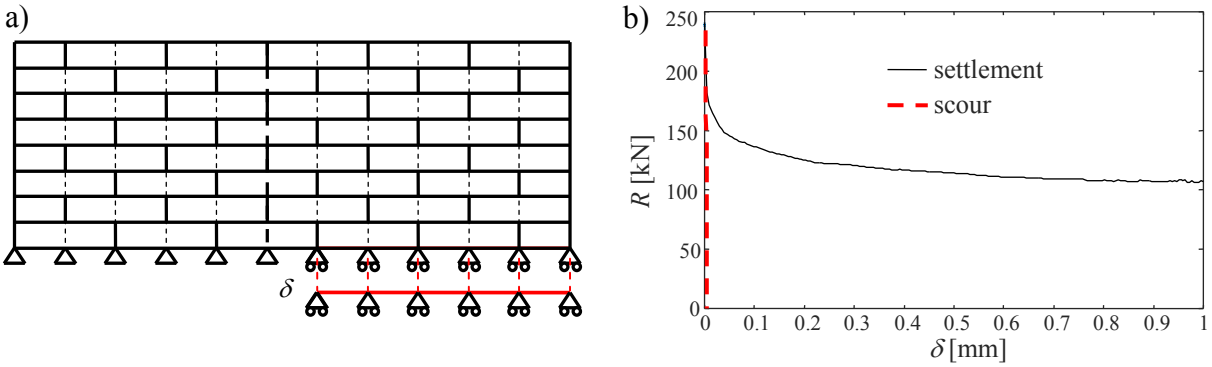

Fig. 7. a) Wall model and support conditions (dotted line for brick-to-brick interfaces, continuous line for mortar interfaces, red line for support interface), b) force-displacement relationship for the case of imposed displacement and force reduction.

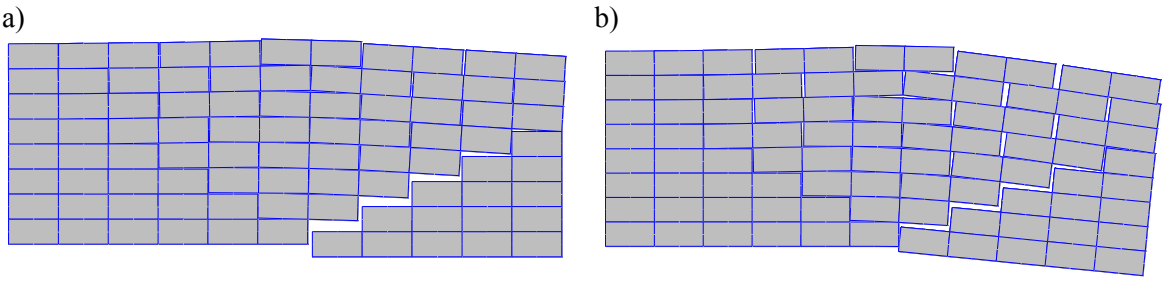

Fig. 8. a) Mechanism in the wall subjected to uniform displacement pattern (a), and scouring process (b). Scale factor 5 for Fig.6a, 50 for Fig. 6b.

4. Numerical simulation of a bridge subjected to scour-induced settlements

This section illustrates the simulation of the experimental test carried out at the Department of Structural and Geotechnical Engineering at the Polytechnic University of Turin [23], [48],[49]. A 2-span masonry arch bridge prototype was first designed taking into account common features, geometric proportions and old design rules of a series of masonry arch bridges. A 1:2 scaled model of the masonry arch bridge was then built in the laboratory. The model has a total length of 5.90 m, a width of 1.60 m and a height of 1.75 m. The two arches are segmental arches with a radius of 2.00 m and an angular opening of 30°. Each span is 2.00 m long between the supports and the thickness of the arch is equal to 0.20 m. The multi-ring arch is built with clay bricks scaled to 130×65×30 mm^3 complying with the adopted

395 modelling scale law and arranged in header bond. The bricks and the mortar are characterised
396 by poor mechanical behaviour to reproduce the typical materials of historical constructions.
397 The mid-span masonry pier was assumed to be placed inside the streambed and its base was
398 subjected to a set of settlements simulating the effects of scour, imposed by means of four
399 independent screws installed at the extremities of the pier base. The masonry pier was cut at a
400 hypothetical middle-height section to allow the insertion of the settlement application system,
401 and an additional weight of 15 kN was added at the bridge top in correspondence of the pier,
402 to simulate the weight of the missing part of the pier. The imposed settlements, corresponding
403 to a roto-translational movement of the pier base, were evaluated by carrying out first
404 hydraulic flume tests on a further scaled down model of the bridge pier and by successively
405 evaluating the evolution of the scour shape through a procedure similar to that presented in
406 Section 2.3. Different tests were carried out by progressively increasing the settlements up to
407 a value of 2.5 mm at the upstream side of the pier base. The observed cracking pattern
408 consists of transversal cracking at the intrados of the arches close to the central pier, and sub-
409 horizontal surface cracking at the physical interface between the arches extrados and the
410 spandrel walls.

411 A finite element model of the bridge is built in ADAPTIC [18] by employing the approach
412 described in Section 2.1. Since the masonry bricks of the arch are arranged in header bond,
413 slippage between the arch rings is not expected, and a single block is considered in the radial
414 direction to model the bricks. In this regard, in [10] it is shown that in the case of bricks
415 arranged in header bond, a detailed representation of masonry bond within the thickness of
416 the arch does not enhance the accuracy but it only increases the computational burden of the
417 analysis.

418 Each arch is modelled by 60 solid elements in the longitudinal direction (i.e., x), and 12
419 elements along the transverse direction, i.e., z, whereas the backfill over the arch is
420 discretised into 12 15-noded elements only along the longitudinal direction, and 8 elements
421 along the transverse direction. The adopted discretisation is characterised by a relatively
422 coarse mesh for the backfill domain when compared to the detailed mesoscale description of
423 the arch which generally leads to savings in the computation time without reducing accuracy,
424 as previously observed in [17] in the analysis of a single-span masonry arch bridge model.
425 The 3D model comprises 1824 20-noded solid elements and 5368 16-noded nonlinear
426 interface elements for the arch and the pier, 2048 15-noded solid elements for the backfill,
427 and the lateral walls, 408 interface elements at the boundary between the arch and the fill.

This corresponds to more than 480000 degrees of freedom which makes the nonlinear analysis of the bridge impractical when using conventional computational resources with a serial code. The model consists of a total of 38 partitions, and the analysis is performed in parallel using 38 processors. The main mechanical properties of the masonry and the backfill materials and spandrel walls are reported in Table 1 and 2. More specifically, masonry compressive strength and Young's modulus as well as tensile resistance and the cohesion for the mortar joints correspond to the values obtained in material tests, which were performed on the same masonry materials used to build the bridge specimen. The other material parameters are typical values used in previous research on masonry arches and bridges [6], [10].

Table 1. Mechanical properties of masonry.

Mortar-Brick interface	Normal stiffness k_N [N/mm^3]	40	Friction angle ϕ_0 [.]	45
	Tangent stiffness k_H [N/mm^3]	17.4	Dilatancy angle ϕ_{d0} [.]	0
	Cohesion c_0 [N/mm^2]	0.28	Mode-I fracture energy GfI [N/mm]	0.1
	Tensile resistance σ_{t0} [N/mm^2]	0.2	Mode-II fracture energy G_{fI}	0.05
	Compressive resistance σ_{c0} [N/mm^2]	4.28	Mode-III fracture energy	0.2
Brick	Elastic modulus E_b [N/mm^2]	5400	Unit weight γ_b [kN/m^3]	19
	Poisson's ratio ν_b [N/mm^2]	0.2		

Table 2. Mechanical properties of backfill and spandrel walls.

Backfill	Elastic modulus E_{bf} [N/mm^2]	200	Friction angle ϕ_0 [.]	60
	Poisson's ratio ν_b [N/mm^2]	0.2	Dilatancy angle ϕ_{d0} [.]	30
	Cohesion c_{bf} [N/mm^2]	0.01	Unit weight γ_b [kN/m^3]	21
Spandrel Walls	Elastic modulus E_{bw} [N/mm^2]	1451	Dilatancy angle ϕ_{d0} [.]	10
	Poisson's ratio ν_{bw} [N/mm^2]	0.15	Compressive Cap I_c [N/mm^2]	4.3
	Cohesion c_0 [N/mm^2]	0.75	Tensile Cap I_t [N/mm^2]	0.13
	Friction angle ϕ_0 [.]	60	Unit weight γ_{bw} [kN/m^3]	19

A time history analysis is performed on the bridge model by imposing increasing vertical displacements at the nodes at the base of the piers. The displacement profile varies linearly along the transverse direction (i.e. z). The nodes at the downstream side of the pier base are assumed fixed, whereas those at the upstream side are subjected to a constant downward velocity of 0.20 mm/s. Fig. 9 shows the deformed shape of the arch bridge model for increasing values of the maximum imposed displacement, together with the plastic

deformations in the backfill. As expected, the plastic deformations in the backfill increase for increasing settlements. In particular, higher plastic deformations are observed at the upstream side of the bridge, with very high values in proximity of the spandrel walls. No plastic deformations are observed in the backfill above the central pier. This is because the vertical patch load applied in that zone increases the resistance of the frictional backfill material.

Fig. 10 portrays the stresses along the longitudinal direction in the bricks.

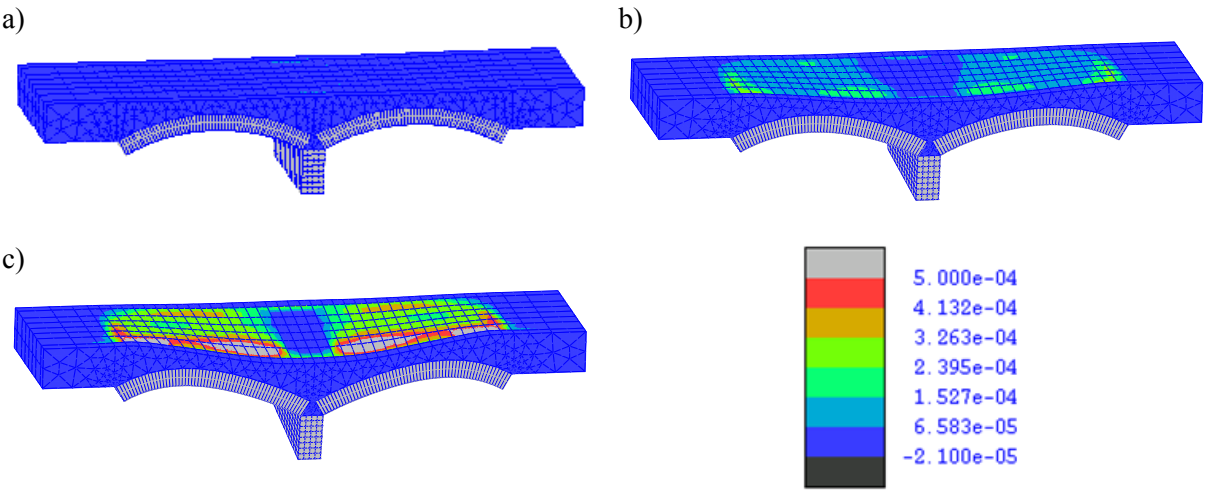

Fig. 9. Von Mises plastic deformations in the backfill for increasing pier base maximum imposed settlements: a) d_{pmax}= 0mm , b) d_{pmax}= 1.25mm, c) d_{pmax}= 2.5mm.

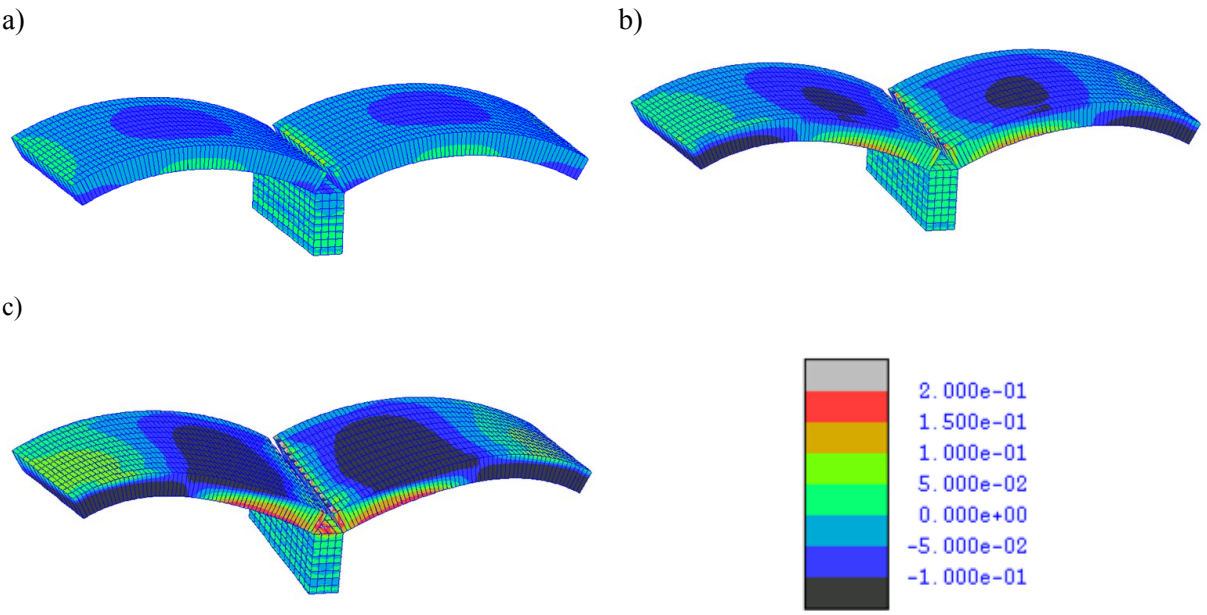

Fig. 10. Stresses (in MPa) along the longitudinal direction in the bricks for increasing pier base maximum imposed displacements: a) d_{pmax}= 0mm , b) d_{pmax}= 1.25mm, c) d_{pmax}= 2.5mm.

Initially, the tension zones are located at the ends of each arch at the extrados, and at midspan at the intrados. The scouring action changes significantly the stress distribution in the arch, by inducing significant tensile stresses at the intrados of the arch, in proximity of the pier on the

upstream side. Moreover, high tensile stresses are observed at the extrados, close to the abutments.

Fig. 11 shows the stresses along the vertical direction (y) in the bricks (a) of the pier, for increasing maximum imposed displacements at the pier base. An initial compression state is observed in the bricks due to permanent loads. However, the differential settlements induce initially a decompression of the upstream side of the pier, and successively tensile stresses. The first tensile stresses are observed for a maximum displacement of 1.25 mm in the upper part of the pier at the upstream side.

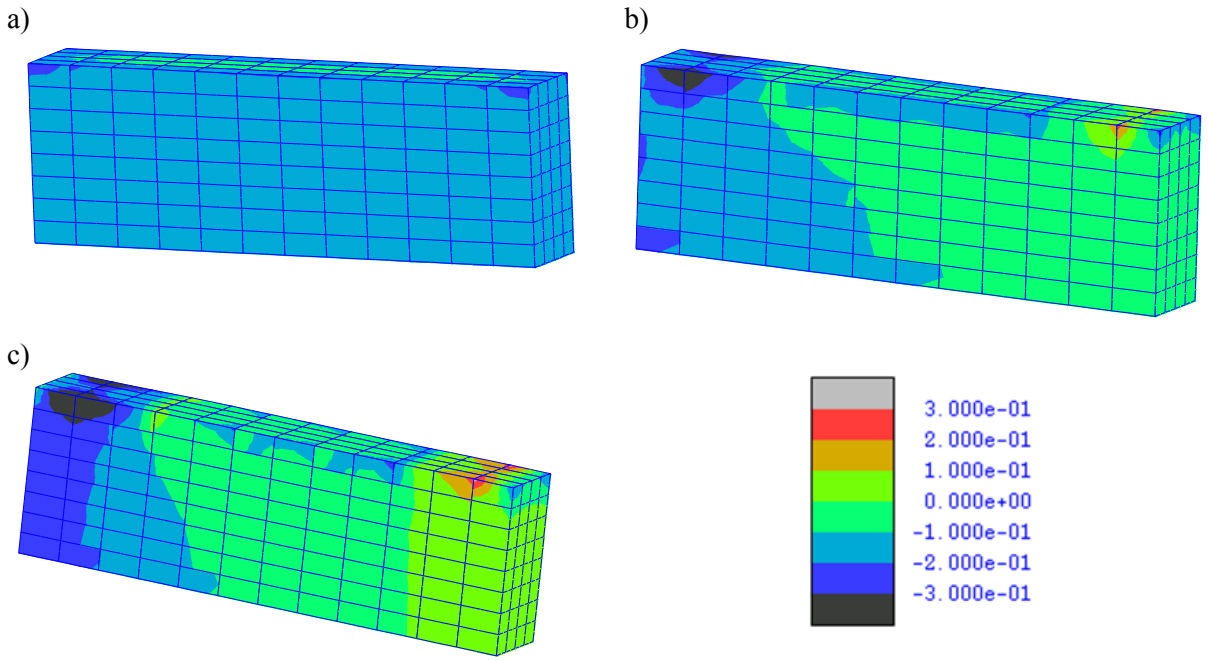

Fig. 11. Stresses along the vertical direction (y) in the bricks (a), and in the interfaces (b), for increasing pier base maximum imposed displacements : a) d_{pmax}= 0mm , b) d_{pmax}= 1.25mm, c) d_{pmax}= 2.5mm.

In the physical test, fibre optic strain sensors were glued on the bridge pier and enabled the measurement of the variation of strains in the bricks along the vertical directions. Fig. 12 shows the strains predicted by the model at the upstream brick surface at the base of the pier, obtained removing the initial compressive strain $\varepsilon_{perm} = -2.88\times10^{-5}$ induced by the bridge permanent loads. Numerical predictions are compared against experimental values showing a good agreement [49]. In the figure, it can be observed that tensile strains start to develop in the bricks at the base of the pier when the maximum displacement of the pier base reaches a value of about 1.8 mm.

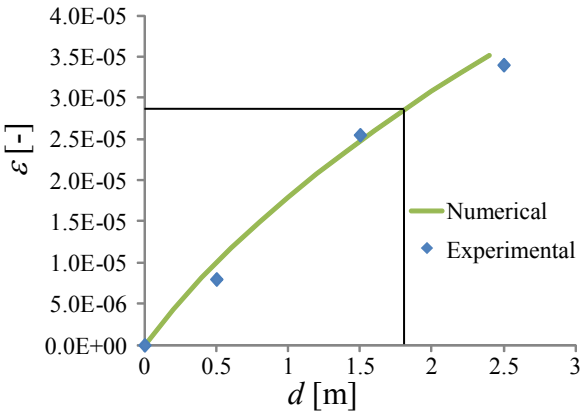

Fig. 12. Brick deformation ε vs. pier displacement: comparison between numerical and experimental results.

Fig. 13 reports the values of the damage parameter in tension and in shear [28] in the mortar interfaces for a maximum imposed displacement of 2.5mm. It is observed that significant tensile damage occurs at the intrados of the arch barrel, close to the central pier, and tensile-shear damage occurs in correspondence of the interface between the arches extrados and the spandrel walls. These zones of damage are consistent with the cracking pattern observed in the experimental test.

a)

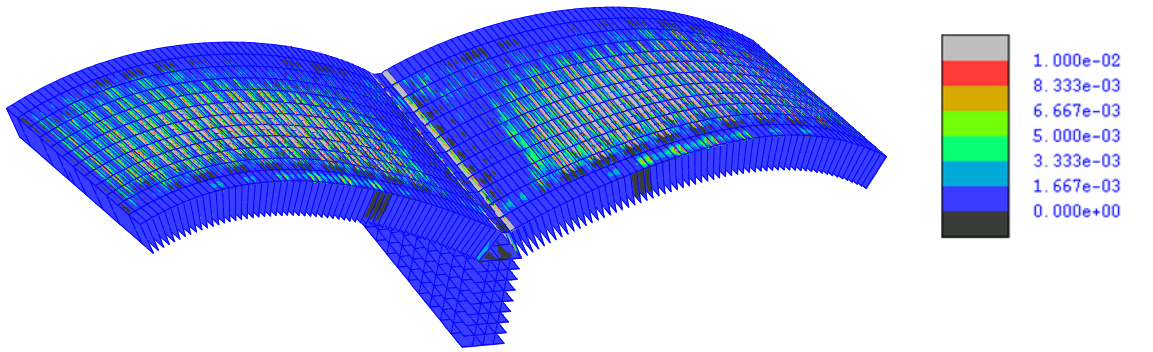

b)

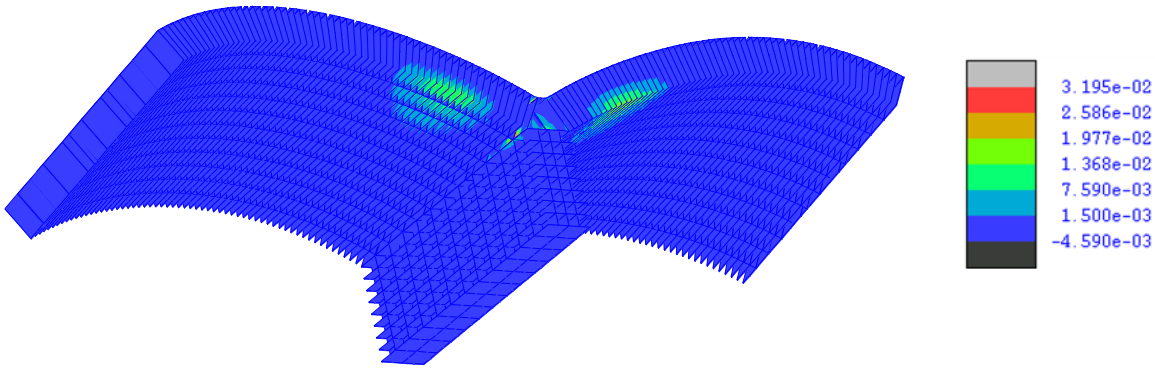

Fig. 13. Values of the damage parameter in shear D_s (a) and in tension D_{nt} (b) of the interfaces of the arch barrel for an imposed pier base maximum displacement of d_{pmax}= 2.5mm.

5. Numerical simulation of the effects of scour on masonry arch bridges on a structure-foundation-soil model

In this section, the strategy for evaluating the effects of scour on masonry arch bridges is applied to a realistic case study, whose geometrical properties are similar to those of many masonry arch bridges in the UK. The analysed structure is a two-span arch bridge with a length of 20.30 m (left to right abutment) and a width along the transverse direction of 3.80 m. The two arches are segmental in shape, with a radius of 9.26 m, a rise of 3.45 m, and a thickness of 0.50 m. The pier has a rectangular transverse section with width of 1.8 m. Fig. 14 reports a schematic illustration of the bridge.

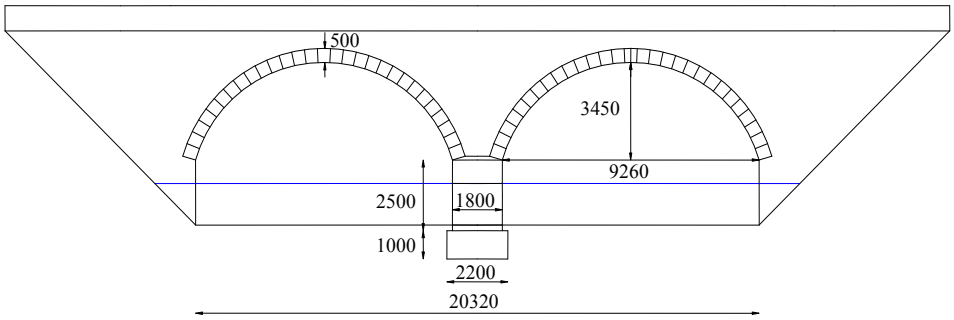

Fig. 14. Schematic illustration of the bridge (dimensions in mm).

The bridge model is analysed under increasing levels of scour until collapse and also under a vertical patch load following the scouring action. The mechanical properties of the model, representative of typical bridge constructions, are reported in Table 3 and Table 4. The riverbed sand is assumed to have a Young's Modulus E_r = 500 MPa and a Poisson's ratio ν_r = 0.15, leading to soil-foundation plinth interfaces with stiffness along the vertical direction k'_{sv} = 0.184 N/mm^3, along the longitudinal $k'_{sh,x}$ = 0.385 N/mm^3, and along the transverse direction $k'_{sh,z}$ = 0.631 N/mm^3 (see Appendix for the computations and Fig. 1 for global axes orientation). Typical values for the friction angle or angle of repose in sands are in the range of 26° to 45° [43]. In this study, ϕ_r is assumed equal to 30°. This value, together with the maximum scour depth y_s (measured from the foundation plinth extrados), controls the shape of the scour hole at the pier base. Scour is assumed not to occur at the abutments.

Each arch is modelled by 28 solid elements in the longitudinal direction (i.e., x), and 6 elements along the transverse direction, i.e., z, whereas the backfill over the arch is discretised into 18 15-noded elements only along the longitudinal direction, and 10 elements along the transverse direction. A finer mesh is employed for the backfill than for the arch barrel along the transverse direction to describe with accuracy the distribution of the stresses

induced by the vertical patch loads applied at the backfill surface. Thus, arch and backfill are modelled independently without mesh compatibility considerations at the physical interface between the two domains and are connected through a non-matching interface tied with the mortar method as proposed in [17]. The total number of degrees of freedom of the model is more than 250000, distributed within 45 partitions.

Table 3. Mechanical properties of masonry.

Mortar-Brick interface	Normal stiffness k_N [N/mm^3]	32.9	Friction angle ϕ_0 [.]	43
	Tangent stiffness k_H [N/mm^3]	14.3	Dilatancy angle ϕ_{d0} [.]	0
	Cohesion c_0 [N/mm^2]	0.1	Mode-I fracture energy G_{fI} [N/mm]	0.05
	Tensile resistance σ_{t0} [N/mm^2]	0.06	Mode-II fracture energy G_{fI}	0.1
	Compressive resistance σ_{c0} [N/mm^2]	8	Mode-III fracture energy	0.5
Brick	Elastic modulus E_b [N/mm^2]	3920	Unit weight γ_b [kN/m^3]	22
	Poisson's ratio ν_b [N/mm^2]	0.15		

Table 4. Mechanical properties of backfill and spandrel walls.

Backfill	Elastic modulus E_{bf} [N/mm^2]	200	Friction angle ϕ_0 [.]	60
	Poisson's ratio ν_b [N/mm^2]	0.2	Dilatancy angle ϕ_{d0} [.]	30
	Cohesion c_{bf} [N/mm^2]	0.01	Unit weight γ_b [kN/m^3]	19
Spandrel Walls	Elastic modulus E_{bw} [N/mm^2]	3100	Dilatancy angle ϕ_{d0} [.]	10
	Poisson's ratio ν_{bw} [N/mm^2]	0.15	Compressive Cap I_c [N/mm^2]	8
	Cohesion c_w [N/mm^2]	0.1	Tensile Cap I_t [N/mm^2]	0.032
	Friction angle ϕ_w [.]	43	Unit weight γ_{bw} [kN/m^3]	22

The procedure outlined in Fig. 6 is followed to evaluate the effect of increasing scour depths. Fig. 15 shows the deformed shape of the bridge at different increasing values of the maximum scour depth y_s. The scour action induces a rotational mechanism at the base of the pier, with non-uniform vertical displacements along the pier base, leading to the formation of a crack between the foundation and the pier.

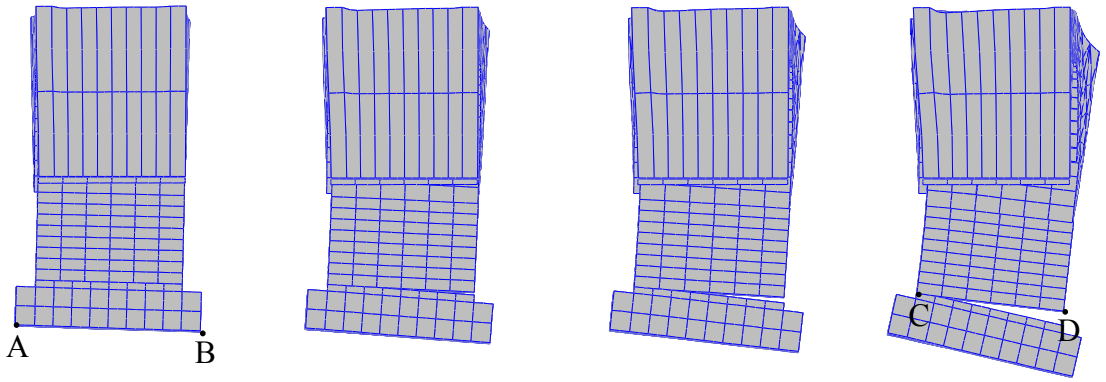

Fig. 15. Deformed shape of the bridge model for increasing levels of maximum scour depth.

Fig. 16a shows the displacements along the vertical direction at the nodes A,B,C and D at the extreme of the foundation and pier base (see Fig. 15), and Fig. 16b the corresponding rotations. The displacements start to increase beyond the values induced by vertical loads only after the maximum scour depth exceeds the foundation depth, i.e. for y_s>1.2 m. The rate of increase of the foundation displacements becomes very significant after the formation of the crack shown in Fig. 15. In fact, after the opening of this crack, the rotation at the base of the foundation reaches values higher than those at the base of the pier.

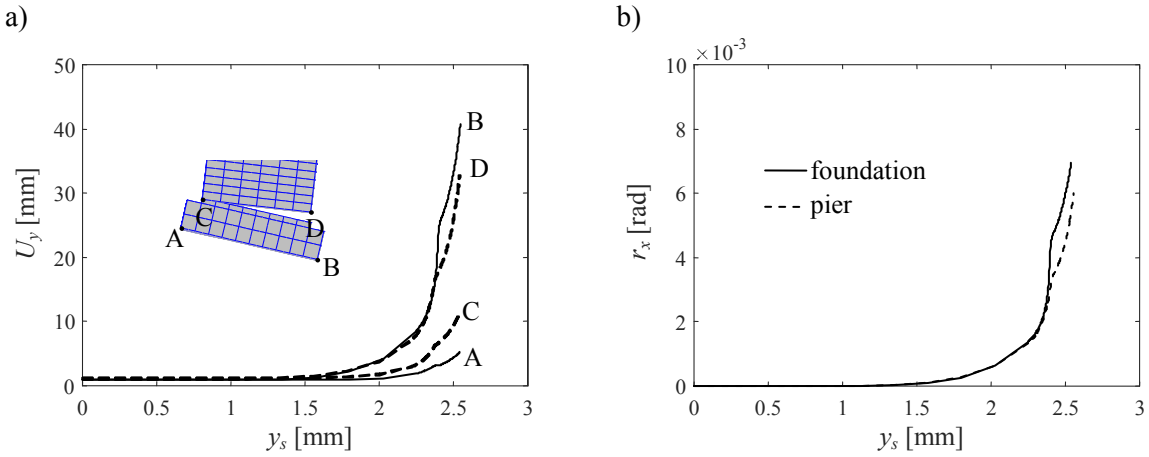

Fig. 16. Displacement (a) and rotation (b) of foundation and pier base for increasing levels of maximum scour depth.

Fig. 17 shows the cracks in the arch barrel for a maximum scour depth y_s = 2.54 m, i.e., 1.34 m below the foundation base. Fig. 18 shows the damage in tension of the mortar interfaces at this scour level.

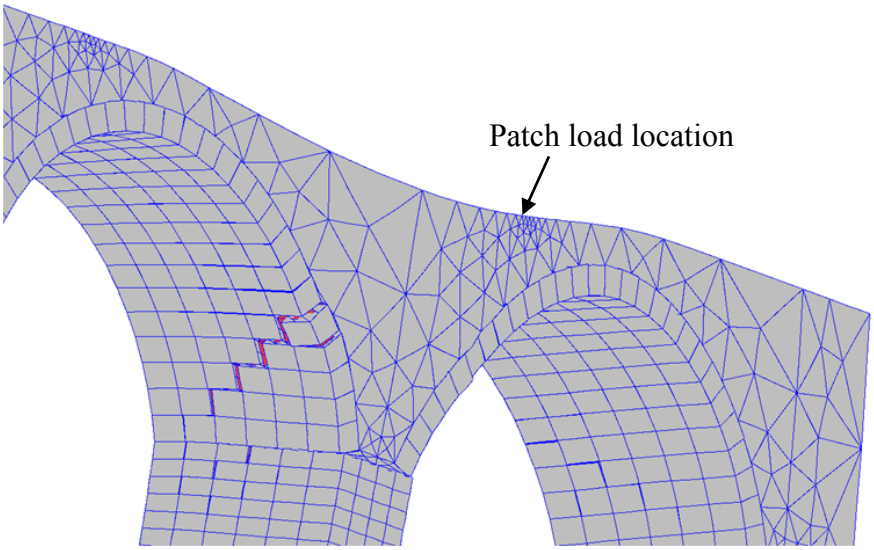

544

545 Fig. 17. Cracking pattern in the arch barrel for maximum scour depth y_s=2.54 m.

a)

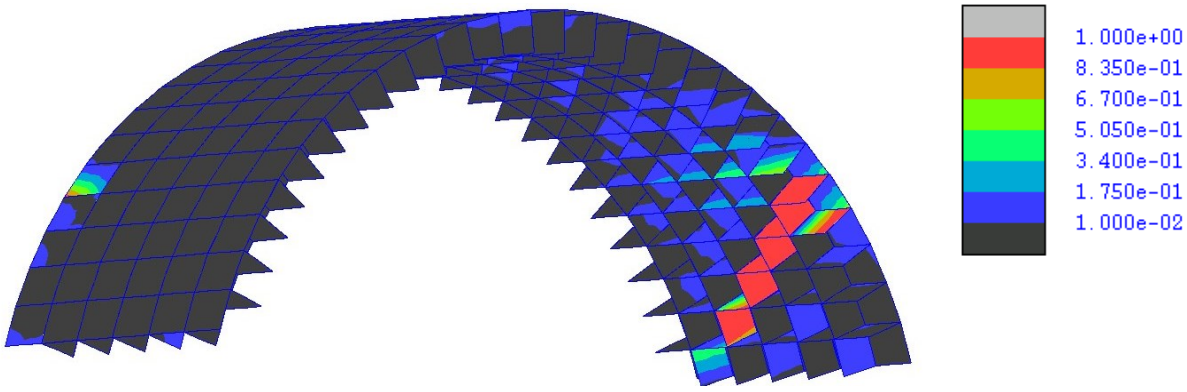

b)

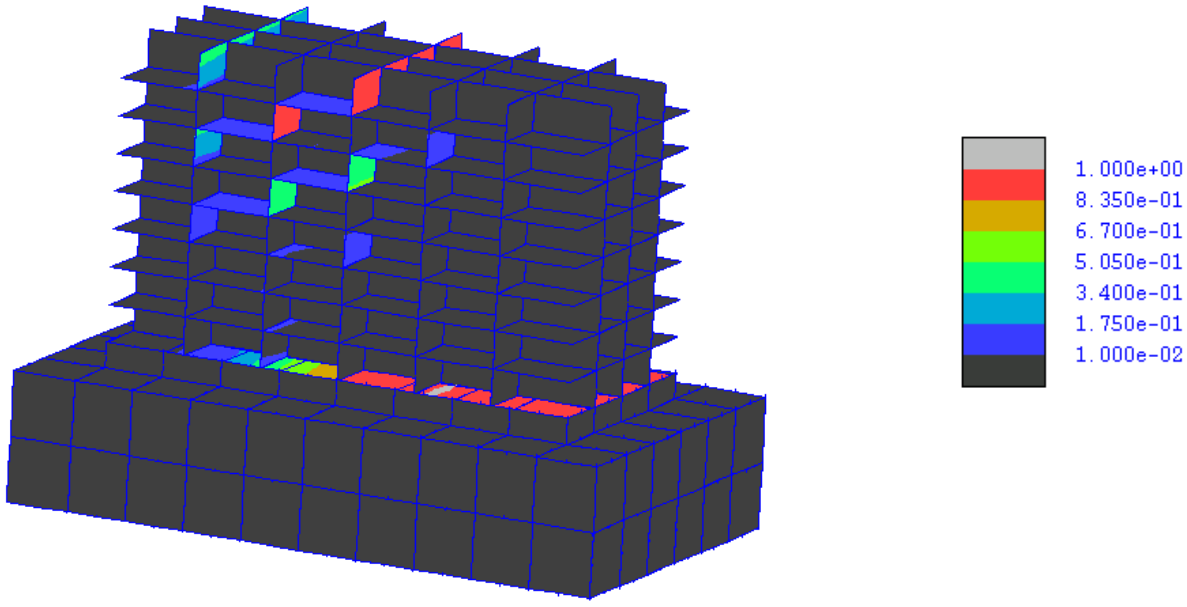

546 Fig. 18. Values of the damage parameter in tension D_{nt} in the arch (a) and the pier (b) for a maximum scour
547 depth y_s=2.54 m.

548 It can be observed that scour induces the formation of both transversal and diagonal cracks in
549 the arch barrel. The diagonal cracks are located in proximity of the pier and also at the
550 abutments, where they are localised at the downstream side. The transversal cracks are
551 localised at midspan of each arch. When the maximum scour depth reaches the value
552 y_s = 2.54 m, the extent of cracking is very significant and the bridge is at collapse. It is
553 noteworthy that a mechanism similar to that described here has been responsible of the
554 collapse of Copley Bridge, a two-span bridge located near Halifax, West Yorkshire, whose
555 geometrical properties are very similar to those of the model considered as case study.

556 In order to evaluate the effect of scour on the capacity of the bridge to withstand traffic
557 loading, the same model is analysed under a vertical patch load of increasing intensity by
558 considering two different conditions: (a) no scour, (b) scour hole with maximum depth y_s =
559 2.1 m. The vertical load is applied at a quarter of the right span, and distributed over an area
560 of dimension 0.52 m and 1.33 m along respectively the longitudinal and transverse direction.
561 A finer mesh is employed for the area of the backfill subjected to the patch load (see Fig. 17).

562 Fig. 19 illustrates the cracking patter at collapse for the two different cases, whereas Fig. 20
563 and Fig. 21 show the corresponding damage in tension and in shear of the interfaces. It can be
564 observed that the collapse mechanism is very similar for both the cases, and it entails the
565 opening of wide cracks at the intrados of the arch barrel, approximately at midspan of the
566 loaded span. In the model subjected to scour prior to the application of the vertical loads, the
567 transverse crack width is higher in correspondence of the upstream side of the pier.

a) b)

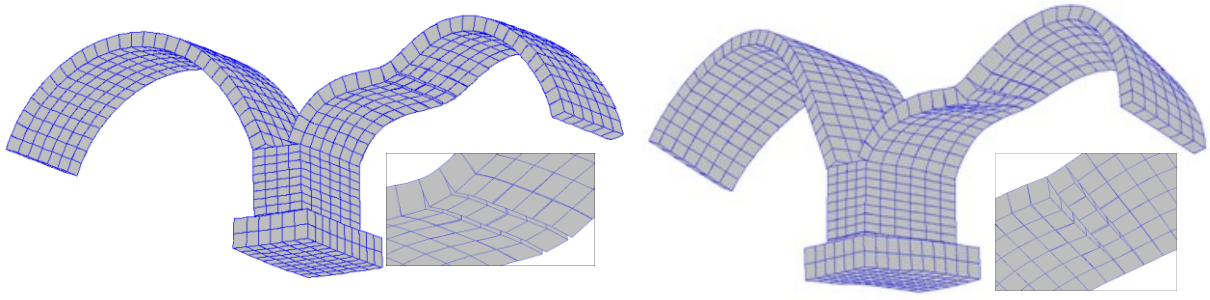

568 Fig. 19. Collapse mechanism for the two loading conditions under vertical load in the case corresponding to no
569 scour (a), and scour maximum depth of 2.1 m (b).

570

571

572

573

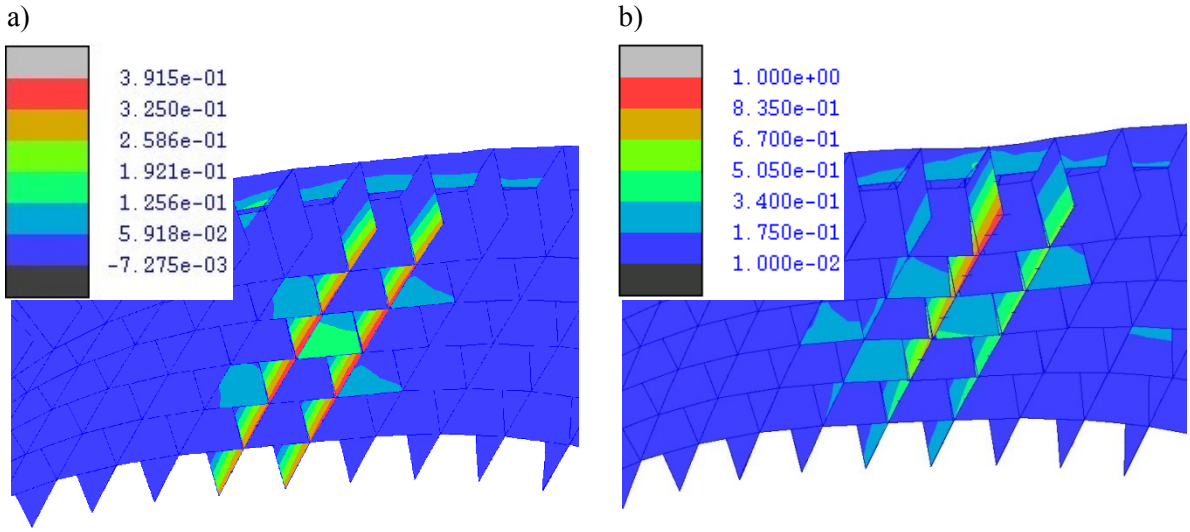

574 Fig. 20. Damage in tension D_{nt} of the mortar interfaces of the arch barrel at collapse under vertical load with no
575 scour (a), and scour maximum depth of 2.1 m (b).

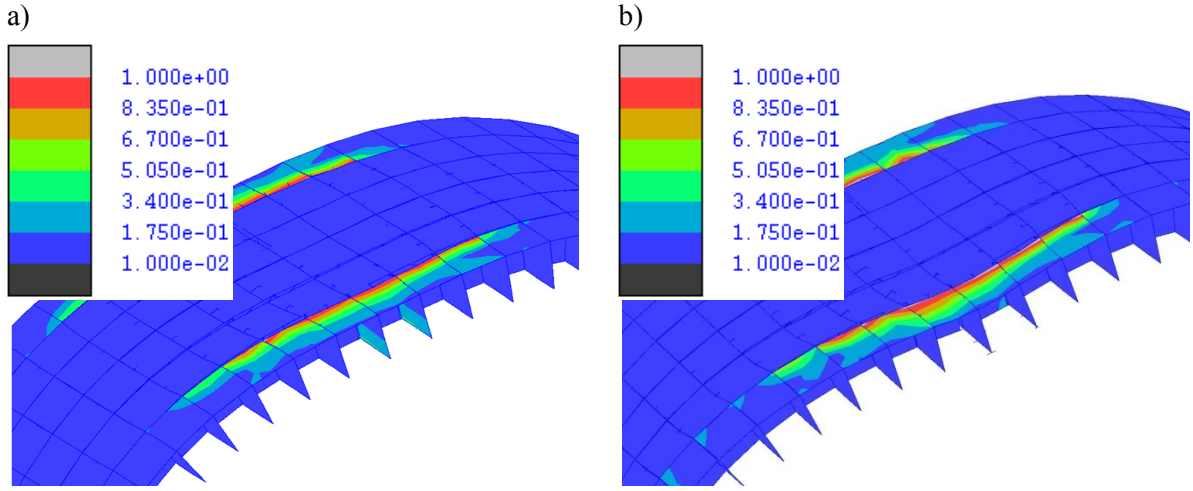

576 Fig. 21. Damage in shear D_s of the mortar interfaces of the arch barrel at collapse under vertical load with no
577 scour (a), and scour maximum depth of 2.1m (b).

578

579 Fig. 22 plots the value of the applied vertical load vs. the displacement of a node of the arch
580 barrel located at quarter span for the two conditions. Both curves pass through the origin, i.e.,
581 they refer to the response after the application of the initial loads (inducing a displacement of
582 1.96 mm of the monitored node) and of the scouring procedure in the case of loading
583 condition (b) (inducing an additional displacement of 2.03 mm).

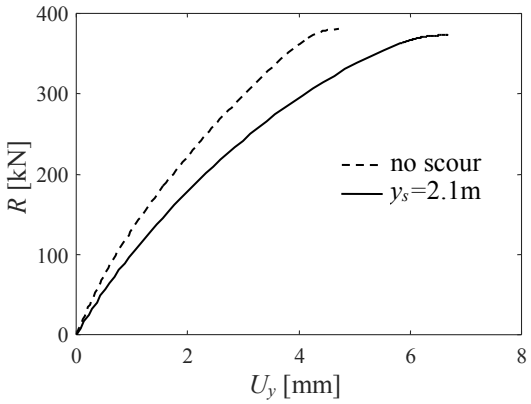

584

585 Fig. 22. Applied vertical load R vs. the displacement U_y of a node of the arch barrel located at a quarter span, for
586 the two conditions of no scour and scour depth y_s = 2.1m.

587 It can be seen that scouring affects significantly the stiffness of the systems. In fact, the
588 secant stiffness to the point at 100 kN is reduced by 32% due to scour. However, the ultimate
589 load, corresponding to the onset of the plateau for the force-displacement curve, is not
590 significantly affected by scouring, since it is equal to 382 kN for the case of no scour, and
591 372 kN for the scoured case. This is due to the high redundancy of the system and the
592 capability of the arch and particularly of the backfill to redistribute the loads, as also
593 evidenced by the collapse mechanisms shown in Fig. 19, which are very similar for the two
594 loading conditions.

595 ## Conclusion

596 This paper has presented a novel strategy for describing the complex three-dimensional
597 behaviour of masonry arch bridges under scour conditions. This strategy allows estimating
598 the levels of scour that lead to the exceedance of different limit states relevant to masonry
599 arch bridge performance. Thus, it contributes to advance current approaches for scour risk
600 assessment which neglect the response of bridges to increasing levels of scour and assume
601 that collapse occurs when the scour depth reaches the foundation level. The proposed
602 modelling approach combines a mesoscale description for masonry arches and piers with a
603 continuum model of the backfill, the spandrel walls, and the foundations. The soil-foundation
604 interaction is described by considering Winkler-type interfaces, which are progressively
605 removed in a time-history analysis to simulate the evolution of the scour process. Non-
606 conforming interfaces between the arch barrel and the backfill and a domain partitioning
607 approach allowing for parallel computation are used to achieve computational efficiency.

Initially, a simple masonry wall with dry bricks has been considered to demonstrate the capability of the proposed model to describe the collapse mechanism induced by the settlement of a part of the wall base. Moreover, a comparison has been performed between the mechanism obtained by imposing a pre-defined settlement pattern and the one obtained by progressively reducing the stiffness of the interfaces supporting the wall base. Successively, the experimental test on a two-span bridge model under scour-induced settlements has been analysed. It has been shown that the proposed model enables prediction of the cracking in the arch and between the arch and the spandrel walls. Finally, the case of a two-span bridge representative of many bridges in the UK is analysed under increasing scour depths, until the collapse condition is attained. The results of the analysis show that scour induces significant reduction of stiffness but the capacity against vertical loading may not be significantly jeopardised, unless very high scour depths are attained, due to the inherent redundancy of the system and the backfill ductile behaviour.

The proposed modelling strategy can be used to perform parametric analyses for different bridge, channel, and scour hole properties. Future studies will investigate the effect of other flood-induced loadings and retrofit strategies for enhancing the bridge capacity against the effect of scour. Together with these numerical studies, further experimental studies should be carried out to investigate the development of the actual scour hole and its effect on masonry arch bridges, as well as to validate numerical models. Moreover, additional research is needed to investigate the interaction between the foundation and the surrounding soil undergoing scour, utilising a more accurate representation than that offered by simplified models based on linear elastic springs.

Acknowledgements

The financial support of the European Commission through the Marie Skłodowska-Curie Individual fellowship IF ("FRAMAB", Grant Agreement 657007) for the first author is greatly acknowledged. The authors also acknowledge the Research Computing Service at Imperial College for providing and supporting the required High Performance Computing facilities.

Appendix

The figures and formula are taken from Figure 4-4 of FEMA 356 [37].

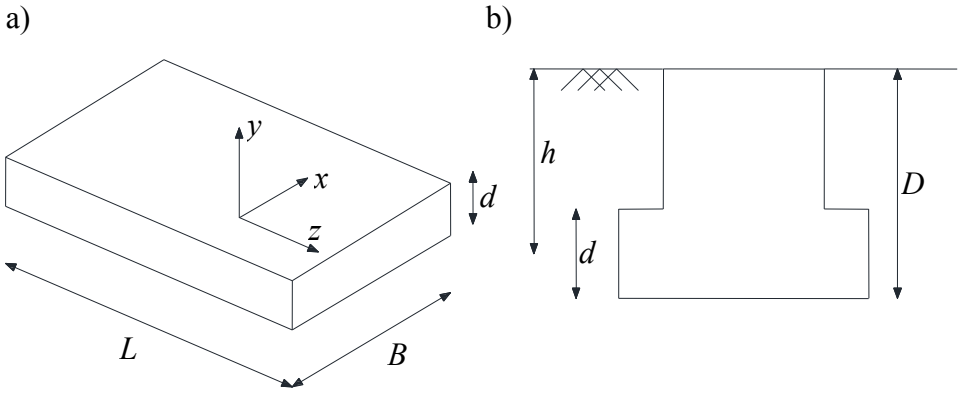

Figure A1. a) Geometrical parameters and local reference system of the foundation, b) geometrical parameters describing foundation embedment.

Table A1. Mechanical and geometrical parameter values.

E [Mpa]	v [-]	G [Mpa]	L [mm]	B [mm]	D [mm]	d [mm]	h [mm]
500	0.2	208.33	4800	2800	1200	1000	700

$$k'_{sv} = \frac{k_{sv}}{A_z} = \frac{1}{BL}\beta_y \frac{GB}{1-v}\left[1.55\left(\frac{L}{B}\right)^{0.75} + 0.8\right] = 0.184 \text{ N/mm}^3$$

$$\beta_y = \left[1 + \frac{1}{21}\frac{D}{B}\left(2 + 2.6\frac{B}{L}\right)\right] \cdot \left[1 + 0.32\left(\frac{d(B+L)}{BL}\right)^{2/3}\right] = 1.0875$$

$$k'_{sh,z} = \frac{k_{sh,z}}{A_x} = \frac{1}{2Bd}\beta_z \frac{GB}{2-v}\left[3.4\left(\frac{L}{B}\right)^{0.65} + 1.2\right] = 0.631 \text{ N/mm}^3$$

$$\beta_z = \left[1 + 0.21\sqrt{\frac{D}{B}}\left(2 + 2.6\frac{B}{L}\right)\right] \cdot \left[1 + 1.6\left(\frac{hd(B+L)}{BL^2}\right)^{0.4}\right] = 1.808$$

$$k'_{sh,x} = \frac{k_{sh,x}}{A_x} = \frac{1}{2Ld}\beta_x \frac{GB}{2-v}\left[3.4\left(\frac{L}{B}\right)^{0.65} + 0.4\frac{L}{B} + 0.8\right] = 0.385 \text{ N/mm}^3$$

$$\beta_x = \left[1 + 0.21\sqrt{\frac{D}{B}}\left(2 + 2.6\frac{B}{L}\right)\right] \cdot \left[1 + 1.6\left(\frac{hd(B+L)}{BL^2}\right)^{0.4}\right] = 1.808$$

References

[1] Page J. Masonry Arch Bridges - State of the Art Review. HMSO, London; 1993.

[2] McKibbins LD, Melbourne C, Sawar N, Gaillard CS. Masonry arch bridges: condition appraisal and remedial treatment, CIRIA Report C656, London, UK: Construction Research and Information Association; 2006.

[3] Transport Committee. The Impact of Flooding on Bridges and Other Transport Infrastructure in Cumbria: Oral and Written Evidence. House of Commons, Great Britain Parliament, 30-03-2010.

[4] Collins J, Steele M, Wilkes D, Ashurst D, Harvey B. Investigation into highway bridge damage and failures during the November 2009 Cumbria flood event. In: Proceedings fifth international conference on forensic engineering, London, 16–17 April 2013.

[5] Kirby AM, Roca M, Kitchen A, Escarameia M, Chesterton OJ. Manual on scour at bridges and other hydraulic structures, second edition (C742), CIRIA; 2015.

[6] Zhang Y. Advanced nonlinear analysis of masonry arch bridges PhD Thesis. London: Imperial College; 2015.

[7] Sarhosis V, De Santis S, De Felice G. A review of experimental investigations and assessment methods for masonry arch bridges, Structure and Infrastructure Engineering 2017;12: 1-19.

[8] Milani G, Lourenço PB. 3D non-linear behavior of masonry arch bridges. Computers & Structures 2012;110-111:133-150.

[9] Gibbons N, Fanning A. Progressive cracking of masonry arch bridges. Proceedings of the Institution of Civil Engineers - Bridge Engineering 2016;169: 93-112.

[10] Zhang Y, Macorini L, Izzuddin BA. Mesoscale partitioned analysis of brick-masonry arches. Engineering Structures 2016; 124: 142-166.

[11] Dikanski H, Hagen-Zanker A, Imam B, Avery K. Climate change impacts on railway structures: bridge scour. In: Proceedings of the Institution of Civil Engineers-Engineering Sustainability, Thomas Telford Ltd; 2016.

[12] Highways Agency. The assessment of scour and other hydraulic actions at highway bridges, BD 97/12, vol 3, section 4, part 21, Design Manual for Roads and Bridges, Highways Agency, UK; 2012.

[13] Chung-Chan H., Wen-Gi Y. Behavior of scoured bridge piers subjected to flood-induced loads. Engineering Structures 2014; 80: 241-250.

[14] Chung-Chan H, Wen-Gi Y, Vulnerability evaluation of scoured bridges under floods. Engineering Structures 2017; 132: 288-299.

[15] Klinga JV, Alipour A. Assessment of structural integrity of bridges under extreme scour conditions. Engineering Structures 2015; 82: 55-71.

[16] Macorini L, Izzuddin BA. A non-linear interface element for 3D mesoscale analysis of brick-masonry structures. International Journal for Numerical Methods in Engineering 2011; 85:1584-1608.

[17] Minga E, Macorini L, Izzuddin BA. Enhanced mesoscale partitioned modelling of heterogeneous masonry structures. International Journal for Numerical Methods in Engineering 2017; 1–22. https://doi.org/10.1002/nme.5728.

[18] Izzuddin BA. Nonlinear dynamic analysis of framed structures PhD Thesis. Imperial College; 1991.

[19] Jokhio GA. Mixed dimensional hierarchic partitioned analysis of nonlinear structural systems, PhD Thesis, Department of Civil and Environmental Engineering, Imperial College London; 2012.

[20] Jokhio GA, Izzuddin, BA. Parallelisation of nonlinear structural analysis using dual partition super elements. Advances in Engineering Software 2013; 60:81-88.

[21] Jokhio GA, Izzuddin BA. A dual super-element domain decomposition approach for parallel nonlinear finite element analysis. International Journal for Computational Methods in Engineering Science and Mechanics 2015;16:188-212.

[22] Portioli F, Cascini L. Assessment of masonry structures subjected to foundation settlements using rigid block limit analysis. Engineering Structures 2016; 113: 347-361.

[23] Ruocci G. Application of the SHM Methodologies to the Protection of Masonry Arch Bridges from Scour. PhD Thesis, Polytechnic University of Torino, Italy; 2010.

[24] Tubaldi E, Macorini L, Izzuddin B, Manes C, Laio F. A framework for probabilistic assessment of clear-water scour around bridge piers. Structural Safety 2017; 69: 11-22.

[25] Macorini L, Izzuddin BA. Nonlinear analysis of masonry structures using mesoscale partitioned modelling. Adv Eng Softw 2013; 60:58-69.

[26] Page AW. The biaxial compressive strength of brick masonry. In: Proceedings of the Institution of Civil Engineers 1981; 71: 893-906.

[27] Fanning PJ, Boothby TE. Roberts BJ. Longitudinal and transverse effects in masonry arch assessment. Construction and Building Materials 2001; 15: 51-60.

[28] Minga E, Macorini L, Izzuddin BA. A 3D mesoscale damage-plasticity approach for masonry structures under cyclic loading. Meccanica (2017). https://doi.org/10.1007/s11012-017-0793-z.

[29] Gilbert M, Melbourne C, Smith C. Discussion of "Assessment of Multispan Masonry Arch Bridges. I: Simplified Approach" by Antonio Brencich, Ugo De Francesco. Journal of Bridge Engineering 2006; 11: 257-259.

[30] Dolarevic S, Ibrahimbegovic A. A modified three-surface elasto-plastic cap model and its numerical implementation. Computers & structures 2007; 85: 419-430.

[31] De Souza Neto EA, Peric D, Owen DRJ. Computational Methods for Plasticity: Theory and Applications. Swansea, Wiley; 2008.

[32] Witzany J, Cejka T. Reliability and failure resistance of the stone bridge structure of Charles Bridge during floods. Journal of civil engineering and management 2007; 13: 227-236.

[33] Witzany J, Cejka T, Zigler R. Failure Resistance of the Historic Stone Bridge Structure of Charles Bridge. I: Susceptibility to Nonstress Effects. Journal of performance of constructed facilities 2008; 22: 71-82.

[34] Terzaghi K. Evaluation of coefficients of subgrade reaction. Geotechnique 1955; 5: 41-50.

[35] Baban TM. Shallow Foundations: Discussions and Problem Solving. Wiley-Blackwell; 2016.

[36] Gazetas G. Foundation Vibrations. In: Foundation Engineering Handbook, Van Nostrand Reinhold, New York, 1991.

[37] FEMA 356. Prestandard and Commentary for the Seismic Rehabilitation of Buildings, American Society of Civil Engineers for Federal Emergency Management Agency, Washington, D.C; 2000.

[38] NEHRP Consultants Joint Venture. Soil-Structure Interaction for Building Structures, Report NIST GCR 12-917-21, Applied Technology Council and Consortium of Universities for Research in Earthquake Engineering for the National Institute of Standards and Technology, Washington, D.C; 2012.

[39] Das BM. Principles of foundation engineering. Cengage learning; 2015.

[40] Zhang L. Nonlinear analysis of laterally loaded rigid piles in cohesionless soil. Computers and Geotechnics 2009; 36: 718-724.

[41] Rodriguez-Villares A. Analysis of large complex masonry structures using nonlinear interface elements and partitioned modelling, Imperial College London; 2014.

[42] Melville BW, Coleman SE. Bridge scour, Water Resources Publications, Highlands ranch, Colorado, USA; 2000.

[43] Hoffmans GJCM, Verheij HJ. Scour manual. Balkema, Rotterdam, Netherlands; 1997.

[44] Link O, Pfleger F, Zanke U. Characteristics of developing scour-holes at a sand-embedded cylinder. International Journal of Sediment Research 2008; 23: 258-266.

[45] Pagliara S, Carnacina I. Temporal scour evolution at bridge piers: Effect of wood debris roughness and porosity. Journal of Hydraulic Research 2010; 48: 3-13.

[46] Baykal C, Sumer BM, Fuhrman DR, Jacobsen NG, Fredsøe J. Numerical investigation of flow and scour around a vertical circular cylinder. Philosophical Transactions of the Royal Society A: Mathematical, Physical and Engineering Sciences 2015; 373: 20140104.

[47] Harris JM, Whitehouse RJS. Marine scour: Lessons from Nature's laboratory. In Scour and Erosion: Proceedings of the 7th International Conference on Scour and Erosion, Perth, Australia, 2-4 December 2014, p. 19. CRC Press, 2014.

[48] Invernizzi S, Lacidogna G, Manuello A, Carpinteri A. AE Monitoring and Numerical Simulation of a Two-span Model Masonry Arch Bridge Subjected to Pier Scour. Strain 2011; 47: 158-169.

[49] Ruocci G, Quattrone A, Zanotti Fragonara L, Ceravolo R, De Stefano A. Experimental testing of a masonry arch bridge model subject to increasing level of damage. In: 4th International Conference on Advances in Experimental Structural Engineering, Ispra; 2011.